3. QPS PHYSICS DESIGN

This chapter describes the physics optimization of the QPS plasma and coil configurations: the optimization approach used to obtain the plasma configuration, the physics design requirements, and the general properties of the QPS reference configuration.

3.1. Integrated Optimization Approach

The QPS reference configuration was determined through a systematic optimization procedure[1-4] that balances **physics requirements** (confinement quality, plasma stability to pressure and current-driven modes, bootstrap current consistency), **design goals** (low aspect ratio, minimum plasma width for good neutral shielding, rotational transform (ι) profile which avoids low order resonances, sizeable ι from coils) and **engineering constraints** (adequate coil-plasma and coil-coil separation, sufficient space in center for an Ohmic heating transformer and toroidal coils).

The low-A_p QPS configuration evolved from a quasi-helical configuration at much higher A_p. During the optimization, as A_p was lowered (from ~5 to ~2.5), it was found that the plasma naturally evolved toward a quasi-poloidally-symmetric state. This was a consequence of requiring the self-consistent bootstrap current to remain small (compared with that in an equivalent tokamak having the same ι profile), together with enforcing an omnigeneity constraint to guarantee adequately low neoclassical transport levels (compared with the anomalous ISS-95 scaling values). The reduction in bootstrap current required during the optimization (needed to give good low-n MHD stability properties and greater configurational invariance with β) produced a configuration which naturally avoided the quasi-axisymmetric state being explored by NCSX. To access the lower end of this range of aspect ratios, it was necessary to lower the number of field periods, N. Keeping A_p/N, ι/N fixed was found to be a useful guide for preserving certain physics features during the configuration optimization. In this way, the lowest A_p achieved (A_p ~ 2.5) was obtained for N = 2. The **physics** consequence of low N is to lower ι in systems with shear in order to avoid low order resonances m ~ N/ι This generally increases transport in configurations which rely on significant poloidal flux for orbit confinement. The **engineering** consequence is to allow the stellarator coils to be "far away" from the plasma surface (on the order of ~a/3) while still generating with modest coil currents the complex helical field needed to produce the external transform and shear of the magnetic field. This coil-plasma separation is the key parameter – which should be maximized – for determining the minimum size of a stellarator reactor based on a compact plasma configuration.

Figure 3.1 illustrates the optimization procedure used to determine a low-aspect-ratio plasma configuration with the desired properties. It starts with an initial assumed configuration (usually at large aspect ratio) and proceeds through the following steps: (1) the 3-D plasma equilibrium is calculated using the VMEC equilibrium code [1]; (2) the computed physics properties are compared with the desired target properties and the difference χ^2 is calculated; (3) the plasma boundary shape and plasma profiles are adjusted; (4) steps (1)-(3) are repeated until no further

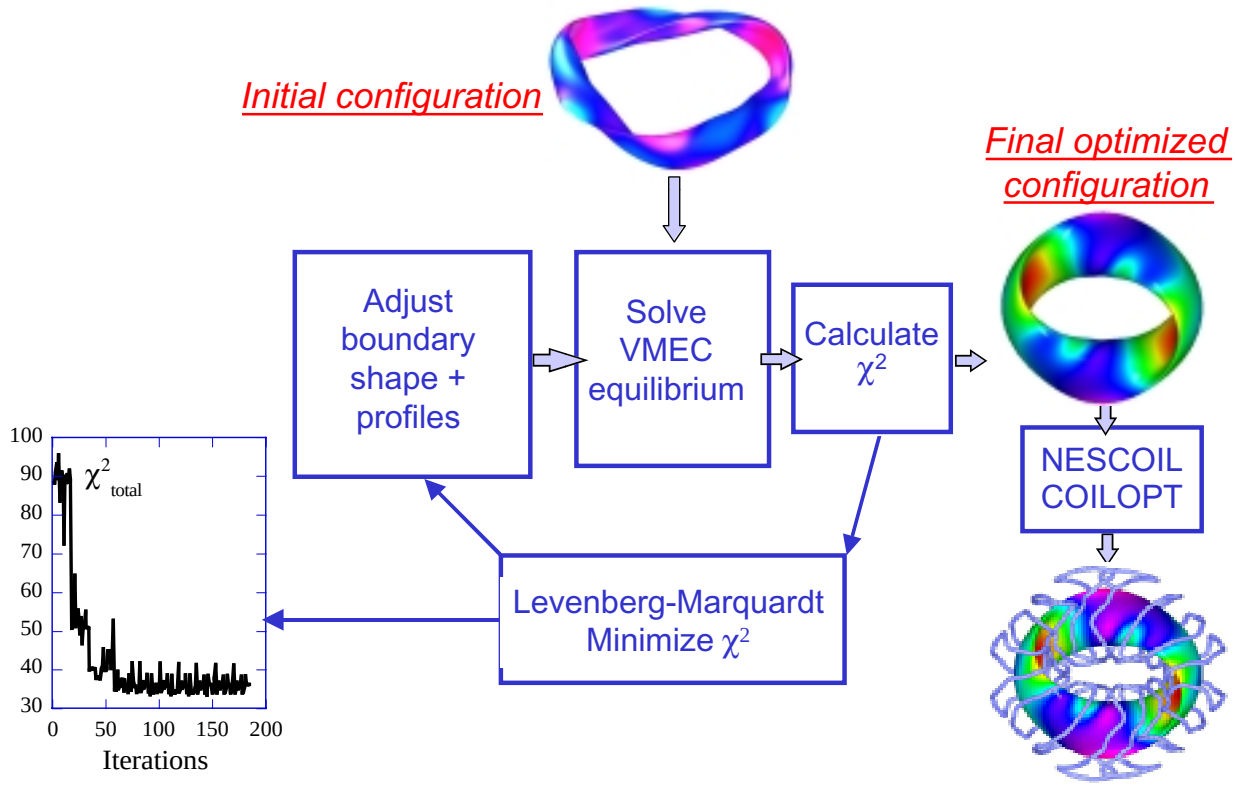

Figure 3.1. The optimization procedure used to find the QPS plasma and coil configuration.

changes in χ^2 occur. A Levenberg-Marquardt scheme is used to minimize χ^2. Typically ~100s iterations through this loop are required and may take several hours of CPU time, depending on the number and type of physics criteria that are computed to evaluate χ^2. The χ^2 measure in the optimization loop is the difference between the desired weighted figures of merit for a particular QPS configuration and that obtained at any stage during the optimization process. Typically, 30-40 Fourier harmonics R_{mn} and Z_{mn}, which describe the shape (R,ϕ,Z) of the last closed flux surface (LCFS), and the expansion coefficients for the pressure and current density profiles (in a Legendre series in the normalized toroidal flux S) are varied in the optimization until the value of χ^2 converges to its minimum value. The optimization process at low aspect ratio proceeds in two steps. Physics optimization criteria, targeting transport and stability properties of the plasma, are initially chosen to find a suitable region of the multi-dimensional phase space (of boundary harmonics) for further exploration. Once such a region is identified, coil and engineering optimization criteria are added as targets to guide the optimization process toward regions of phase space where a realizable set of coils for QPS might exist at these low aspect ratios. The optimized configuration depends on the particular choice of physics and engineering targets and the relative weighting among these. After such an optimized plasma configuration is found, a set of coils is then determined that accurately recreates the desired LCFS, as discussed in Section 3.4. Targeting engineering criteria already at the *physics* optimization level helps to guarantee that a set of coils with reasonable current densities and geometric parameters can be generated.

3.2. Physics Design Requirements

The optimization process successfully integrates a complex, interacting set of physics and engineering criteria. Because of the nonlinear dependence of these "target" criteria on the independent boundary variables, it is often necessary for human judgment to intervene during the optimization in order to guide the process towards an interesting physical state. This intervention typically takes the form of changing the relative weights on the various (often competing) physics criteria in order to eliminate local minima in the χ^2 topography.

A list of physics and engineering targets that can be targeted for optimization and their quantitative measures are given in Table 3.1. The first three targets are related to transport improvement. The alignment of constant B_{min} and J (longitudinal adiabatic invariant) contours with flux surfaces is used to minimize the direct loss of trapped particles. The alignment of

Table 3.1. Physics and engineering targets used in the optimization procedure

Targets (Physics/Engineering)	**Example**
Bounce-average omnigeneity (drift surfaces and flux surfaces aligned)	$B_{min} = B_{min}(\psi)$ $B_{max} = B_{max}(\psi)$ $J = J(\psi)$
Target nearby quasi-symmetries	Minimize B_{mn} if $m \neq 0$ (QP), or if $m/n \neq 1$ (QH)
Local diffusive transport	D, χ from DKES
Current profile	self-consistent I_{BS}, $I(\psi)$ goes to 0 at edge
Limit maximum plasma current	e.g., $I_{max} < 80$ kA
Iota profile	$i(\psi) = 0.25$ ($\rho = 0$) 0.4 ($\rho = a$)
Magnetic Well, Mercier	$V'' < 0$, $D_M > 0$ over cross section
Ballooning stability	$\langle\beta\rangle \sim 2$-4%
Aspect ratio	$R_0/a \approx 2.5$ to 3.5
NESCOIL targets/feasible coil design	Complexity, B_{err}, Max. current density
Adequate shielding of neutrals	Minimum "waist" thickness
Fit within vacuum bell jar	$R_{max} < 1.5$ m
Limit outer surface curvature	avoid strong elongation/cusps

constant B_{max} contours with flux surfaces improves confinement of transitional (i.e., near trapped-passing boundaries) particles. Targeting nearby quasi-symmetries improves confinement of all particles, but can generally only be achieved in an approximate sense. Targeting of transport coefficients in the Drift Kinetic Equation solver, or DKES code [2] is done for a few surfaces (3 - 5) in the "collisional" transport regime ($\nu_* > 1$) where calculations can be performed rapidly. However, this target often lowers transport rates in more collisionless regimes as well and shows good correlation with (post-process) Monte Carlo analysis.

The next three targets deal with current and iota profiles. We try to maintain good alignment between the plasma current profile used in the equilibrium calculation and that predicted by collisionless bootstrap theory. Our design goal for the concept exploration experiment has also been to supply a large fraction of the rotational transform from coils for good equilibrium robustness. For this reason, during the optimization upper limits are placed on the amount of plasma current. The current is usually required to go to zero at the plasma edge along with the pressure profile. We have found that finite edge currents arising from edge pressure gradients (associated with a pressure pedestal, for example) can significantly increase the ballooning stability limits in QPS without destabilizing external kinks. However, the stability limits reported here were conservatively calculated for pressure profiles without such edge gradients, since the properties of QPS plasmas have not been heretofore experimentally examined. Iota profiles are targeted to avoid the major low order rational resonances when possible and to have significant shear otherwise. For our CE designs we have targeted stellarator-like iota profiles. These also provide passive stabilization of neoclassical tearing instabilities for the direction of bootstrap current which characterizes the CE devices.

The next two targets relate to stability. We attempt to maintain a magnetic well and stability to Mercier modes, except near rational surfaces where the Mercier criterion may become unstable over very isolated radial regions. Ballooning stability is targeted using the COBRA code [3] which can very rapidly evaluate ballooning eigenvalues. In addition to varying the outer surface shape , this target can also vary the plasma pressure profile to improve ballooning stability.

The final five targets control geometric properties of the configuration (aspect ratio, minimum "waist", or thickness, of the plasma, overall size and maximum outer surface curvature) and ease of coil design. We have found it necessary to target minimum plasma thickness and surface curvature due to the fact that some of our optimizations (especially when heavy weight is placed on transport and ballooning targets) led to very narrow width flux surfaces and flux surfaces with sharp tips. The coil targets are obtained by running the NESCOIL code [4] to obtain surface current solutions for coils at a fixed displacement from the outer flux surface of the plasma. Targets based on this current sheet include the coil complexity (analytic measure of the smoothness of the coils) and current density We have found that optimizing these parameters of the *sheet current* solution leads to subsequent improved *filamentary* coil designs obtained from the COILOPT calculation.

3.2.1. Transport optimization.

Typical transport targets include the degree of quasi-poloidal symmetry and the L11 Onsager transport coefficient computed using the DKES code. At collisionalities slightly higher than required for the onset to the $1/\nu$ regime, L11 can be obtained rapidly, and it is therefore feasible to include the DKES calculation within an optimization loop. A good correlation between the DKES results for L11 and Monte Carlo calculations is typically obtained for the QPS configurations we have studied. This allows the DKES calculations to be used as a suitable guide for improving thermal confinement, in spite of the neglect of non-local radial drift effects in the DKES code.

Part of the transport optimization process is the determination of a bootstrap current that is approximately consistent (at or near reactor collisionalities) with the internal equilibrium stellarator current. Departures from this consistency will require driven currents. The bootstrap current is calculated in terms of the transform (ι) and pressure profiles, and it depends sensitively on the $|B|$ spectrum. This "bootstrap" consistency turns out to be a fairly limiting constraint on the stability properties of the plasma at finite β. However, not requiring the bootstrap current to vanish (as in W7-X), but merely to be small compared to the equivalent tokamak value, allows for some additional flexibility during the optimization process. In addition, the sign of the bootstrap current should be consistent with the shear of the transform to promote reduction of magnetic islands widths (island healing) and stabilization of neoclassical tearing modes.

3.2.2. Stability optimization.

To avoid low-order resonances, $\iota/N \leq 0.2$ was required in the optimization for the highest $\beta \sim 2\%$ considered for the CE. Two configurations (GB4_NES12B, D) with different ι profiles (Figure 3.2) satisfying this criterion were considered during the optimization procedure. These configurations differ primarily in the amount of shear present in the transform profile, although both satisfy the neoclassical tearing mode stability criterion. The configurations corresponding to these profiles were Mercier stable over the entire plasma volume (with the exception of a few isolated resonances, and very near the magnetic axis for the "high" shear case), as shown in Figure 3.3 (here positive values are stable). The QPS configurations have a substantial magnetic well (favorable average curvature due to both helical curvature and a small Shafranov shift) over the entire plasma cross section and are stabilized primarily by the well rather than the shear (bending) terms in the Mercier criterion (Figure 3.4). This applies even to the "high" shear (reference) configuration, except near the edge, where the destabilizing geodesic curvature is small anyway. The terms arising from the parallel bootstrap current are stabilizing but small. The strong well stabilization implies that high-n resistive modes should also be stable in these configurations.

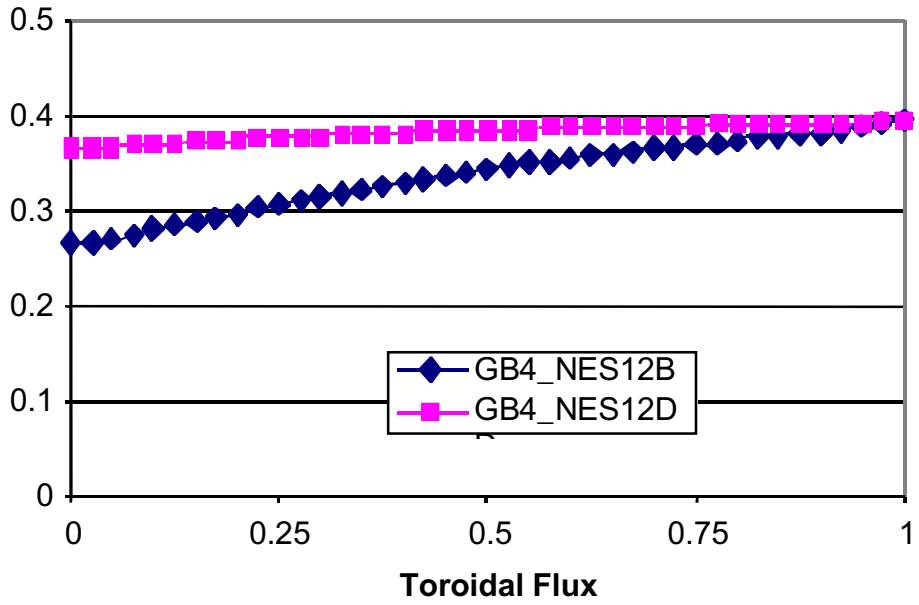

Figure 3.2. Comparison of ι profiles for (B) "high" shear and (D) "low" shear QPS configurations.

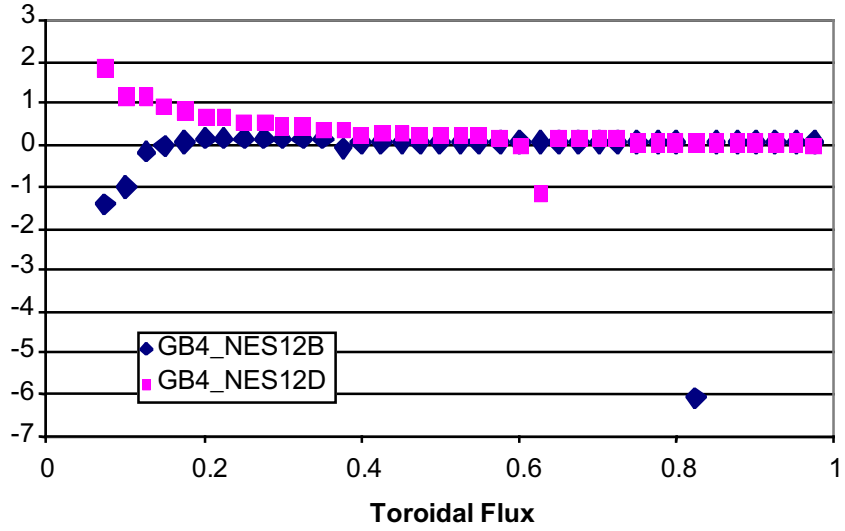

Figure 3. 3. Mercier criterion for (B) "high" shear and (D) "low" shear QPS.

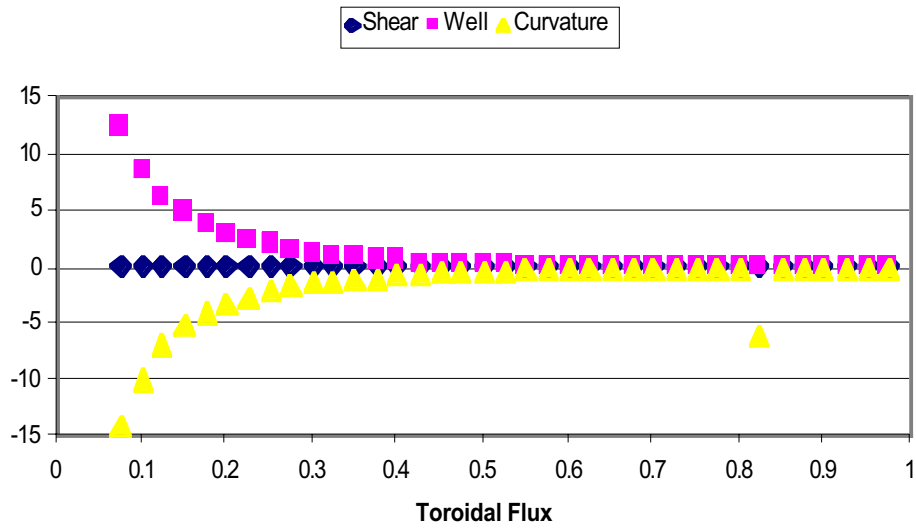

Figure 3. 4. Shear, Well, and Geodesic Curvature contributions vs. radius for the "high" shear (B, top) and "low" shear (D, bottom) QPS configurations.

The COBRA ballooning code [3] allowed us to rapidly evaluate high-n stability (ballooning) during the optimization procedure. It uses a combination of variational methods with quartic mesh extrapolation (Richardson's method) to achieve, for a predefined accuracy, computational speeds 10-100 faster than previously available for three-dimensional systems. The ballooning growth rates vs. the radius for the (B) "high" shear and (D) "low" shear cases are shown in Figure 3.5. The pressure profiles for the cases shown in Figure 3.5 have been optimized for ballooning stability.

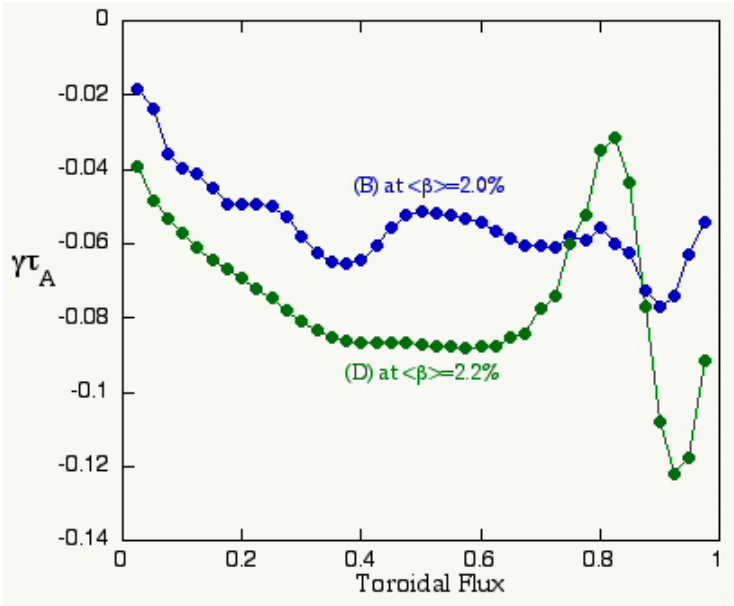

Figure 3. 5. Ballooning growth rates from COBRA for the (B) "high" shear and (D) "low" shear QPS configurations.

Finally, the computed self-consistent bootstrap currents in QPS for $\langle\beta\rangle < 5\%$ are sufficiently small so that low-n modes (kink, vertical displacement mode) are completely stable.

3.3. General Properties of the QPS Reference Configuration

The QPS reference configuration (GB4) is a two-field-period stellarator with $R/a = 2.6$, $R = 0.9$ m, $\langle a \rangle = 0.35$ m, $\langle B \rangle = 1$T, and plasma volume = 2.1 m^3. Figure 3.6 shows top and side views of the last closed flux surface (LCFS) at $\langle\beta\rangle = 2\%$ where the color shading indicates the 2.66:1 variation of |B| on that surface. Here magenta indicates the lowest |B| value and red the highest. The most evident features are the two-field-period symmetry, the general poloidal banding of the |B| contours, the helical magnetic axis, and the sharp ridge with a twist opposite to that of the magnetic axis. Departures from the poloidal closure of the |B| contours indicate the departure from quasi-poloidal symmetry (which is significant at the plasma edge). A better view of the high-field inside end regions can be seen in the oblique view of the LCFS in Figure 3.7. The magnetic field variation through the plasma is illustrated in the horizontal equatorial cross section shown in Figure 3.8.

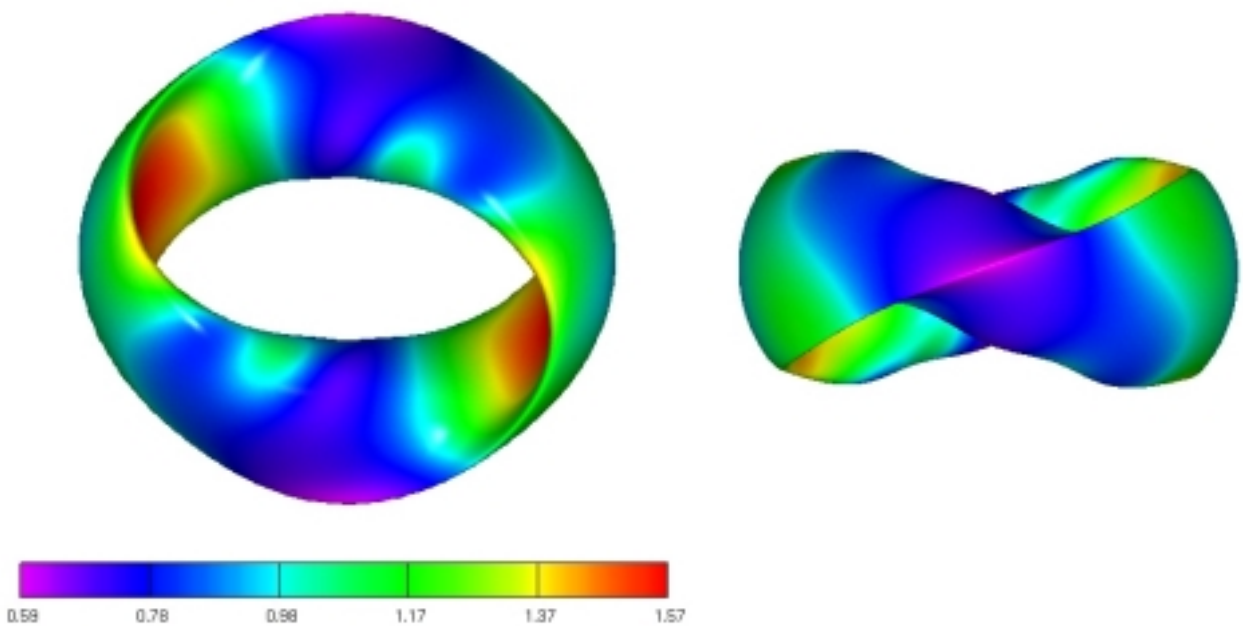

Figure 3. 6. Top and side views of the outer magnetic flux surface for the reference QPS configuration with |B| contours indicated by the color shading.

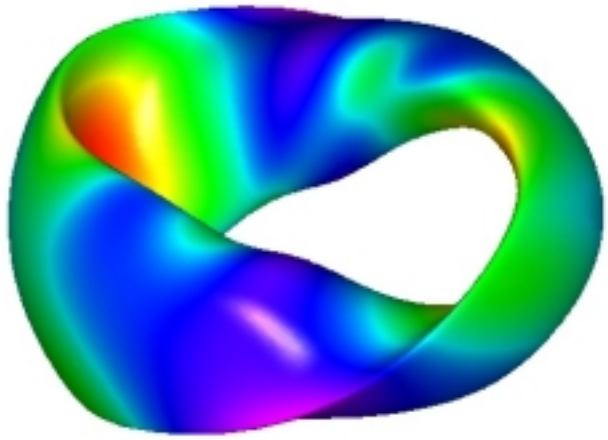

Figure 3.7. An oblique view of the LCFS for the reference QPS configuration.

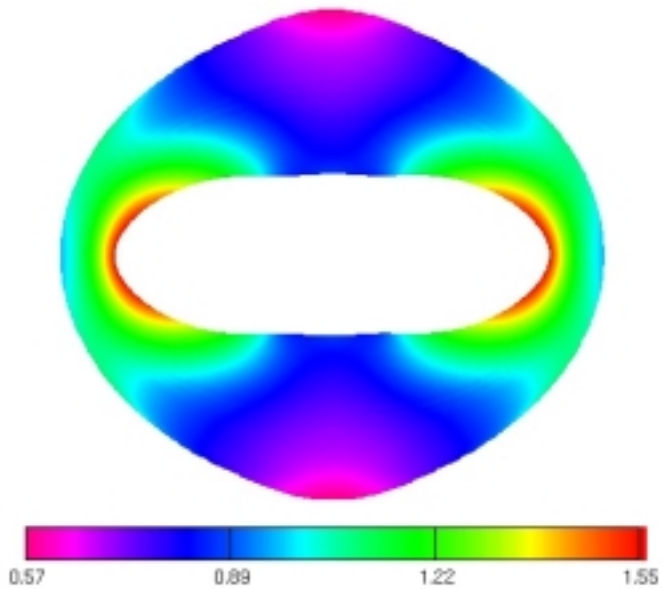

Figure 3. 8. Magnetic field variation in QPS reference configuration on an equatorial plane cut.

The cross section of the plasma varies from bean-shaped to comma-shaped to triangular from the beginning of a field period to halfway through it, as shown in Figure 3.9. These cross sections show the helical excursion of the magnetic axis and the ridge of the LCFS as it moves toroidally from the tips of the "bean" (normalized toroidal angle v = 0) to the end of the "comma" (v = 1/4) to the tip of the "triangle" (v = 1/2) cross sections. The outward shift of the magnetic axis is evidence of the magnetic well.

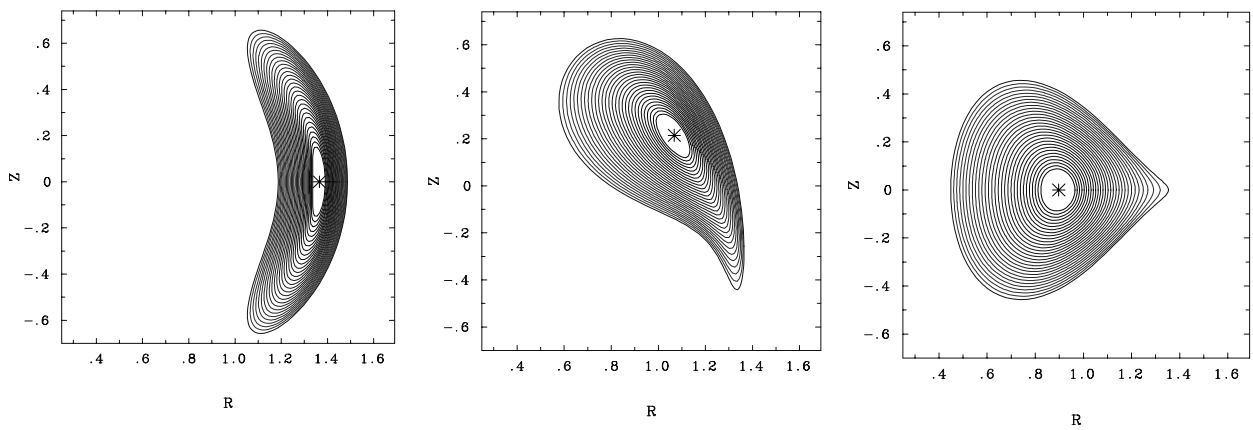

Figure 3.9. Nested magnetic flux surfaces for the QPS reference configuration at three toroidal angles: v = 0, 1/4, and 1/2.

The approximate quasi-poloidal-symmetry of the QPS configuration can be seen by displaying contours of constant |B| values on a flux surface. The appropriate coordinates for this are "Boozer" flux coordinates [5]. In this coordinate system the magnetic flux surfaces are concentric toroids and the magnetic field lines are straight lines in a θ–ϕ plane. The magnitude of the magnetic field can be expressed in a Fourier series in terms of these coordinates as:

$$|B| = \Sigma\, B_{mn}(\psi) \cos\,(m\theta - n\phi)$$

where θ and ϕ are poloidal and toroidal angle variables in "Boozer" coordinates and ψ is the toroidal flux. The magnitude of |B| varies more weakly in the poloidal direction than in the toroidal or radial directions, as shown in Figure 3.10. The degree of quasi-poloidal symmetry decreases on a flux surface in the QPS reference configuration in going from the plasma interior to the edge, as shown in Figure 3.11. Figure 3.12 shows the radial variation with $\rho = \psi^{1/2} \sim r/a$ of the largest terms in the Fourier expansion of |B|. The $m = 0$, $n = 0$ term is just the average magnetic field on a flux surface. This component increases weakly with ρ; this behavior becomes more pronounced for the high-$\langle\beta\rangle$ QPS configurations and aids in providing energetic particle confinement. The next largest term is the bumpy ("linked-mirror") $m = 0$, $n = 1$ component, which dominates especially near the magnetic axis $\rho = 0$. The relative size of the components of |B| which break quasi-poloidal symmetry is given by the B_{mn} terms with $m \neq 0$. The primary deviations from quasi-poloidal symmetry arise from the $1/R$ ($m = 1$, $n = 0$) and helical ($m = 1$, $n = 1$) components near the plasma edge. The QPS magnetic configuration is similar to W 7-X in this respect, but at a factor of 4 smaller aspect ratio.

The QPS reference configuration was optimized at $\langle\beta\rangle \sim 2\%$ including the self-consistent collisionless bootstrap current. However, we have constrained the optimization to provide most of the rotational transform from external coils. At $\langle\beta\rangle \approx 2\%$ the reference QPS configuration has about 60 kA of bootstrap current ($B = 1$ T, $R = 1$ m). Figure 3.13 compares the rotational transform profiles at full β and in vacuum ($\beta = 0$), i.e., with and without this level of bootstrap current. The iota profile maintains a similar shape and decreases by less than ~25% when the

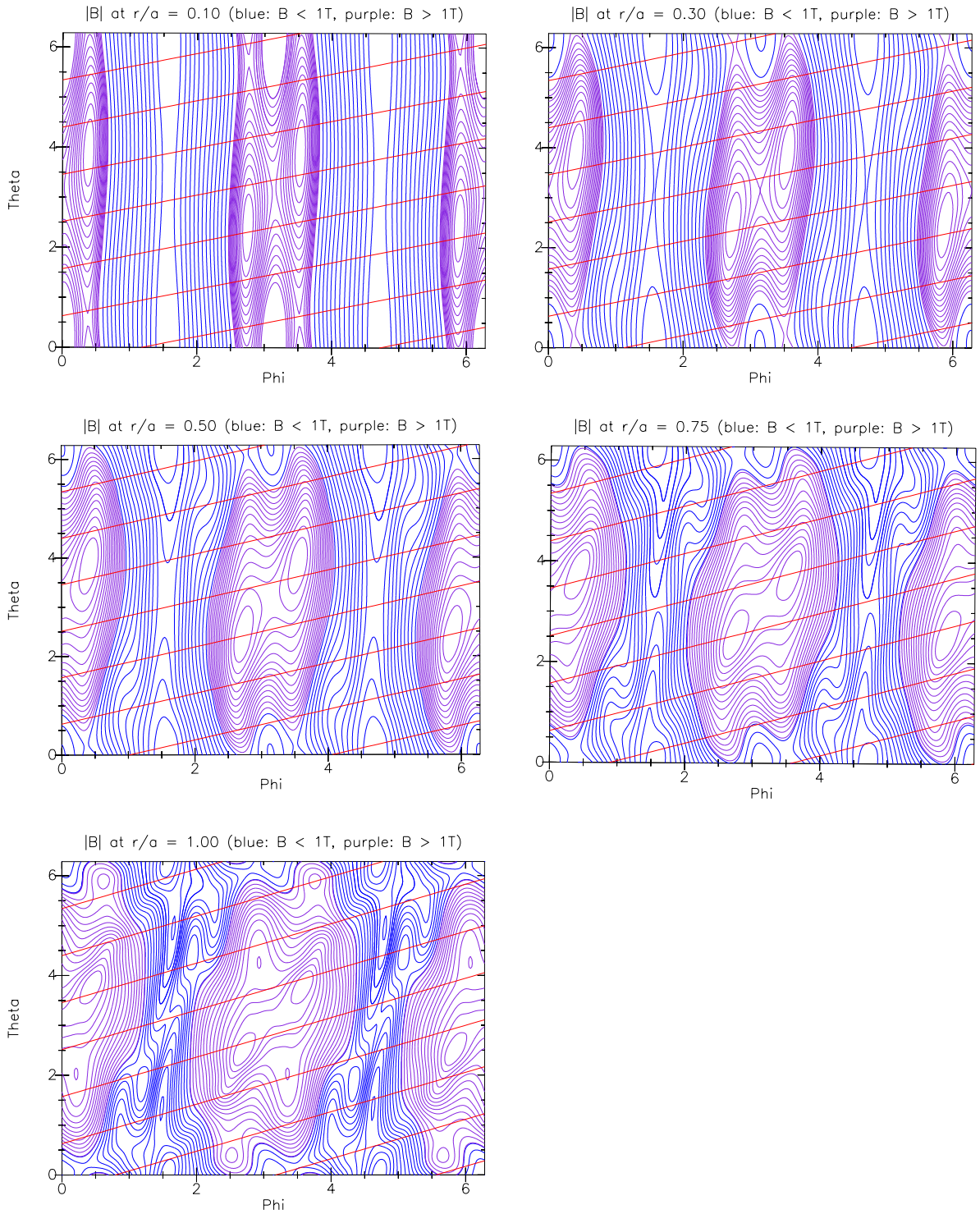

Figure 3.10. Contour plots of |B| vs. poloidal and toroidal angles in Boozer coordinates for r/a = 0.1, 0.3, 0.5, 0.75, and 1.0. The magnetic field lines are shown in red.

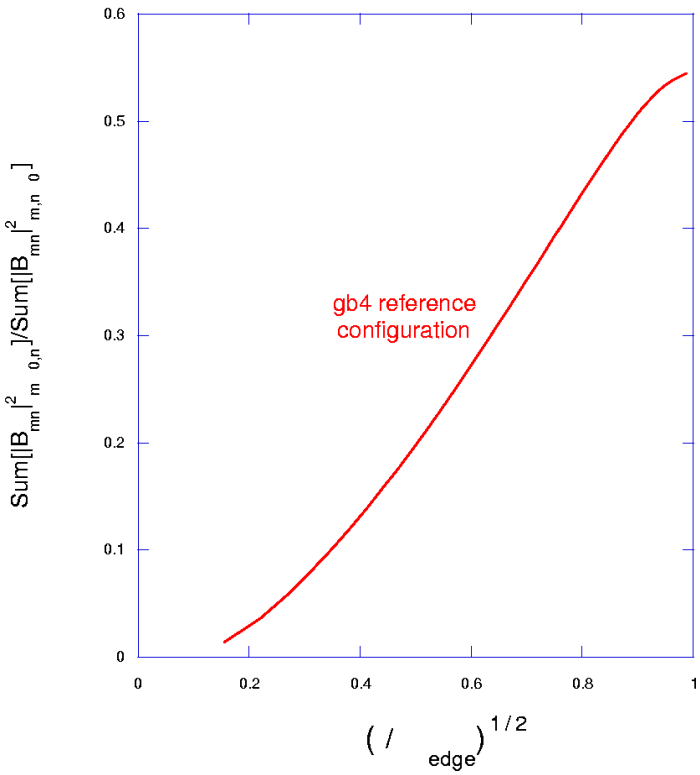

Figure 3.11. Ratio of magnetic energy in non quasi-poloidal modes to that in quasi-poloidal modes vs. ρ.

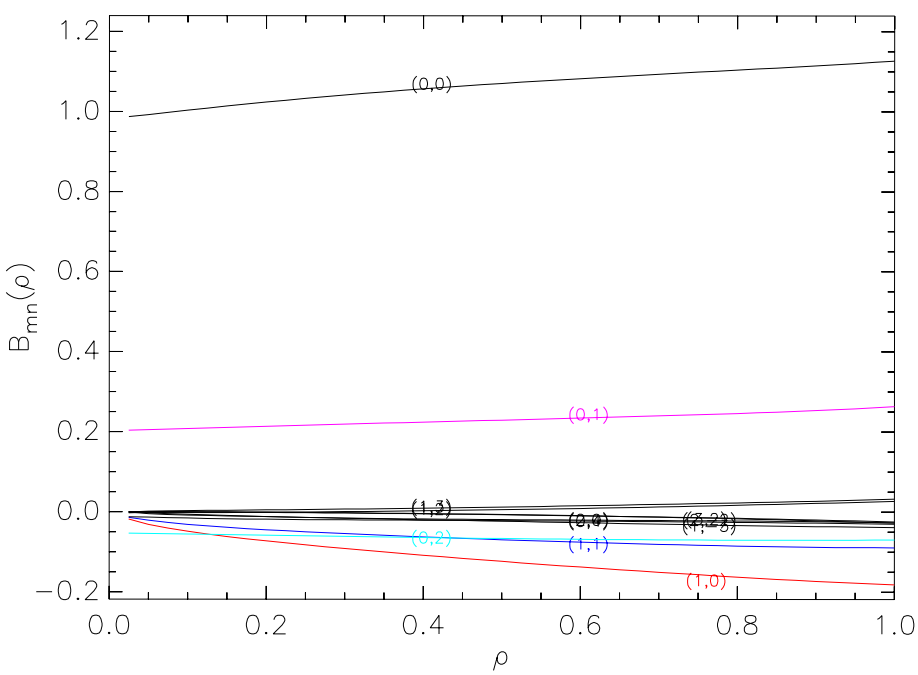

Figure 3.12. Spectrum of $B_{mn}(\rho)$ vs. ρ for the reference configuration.

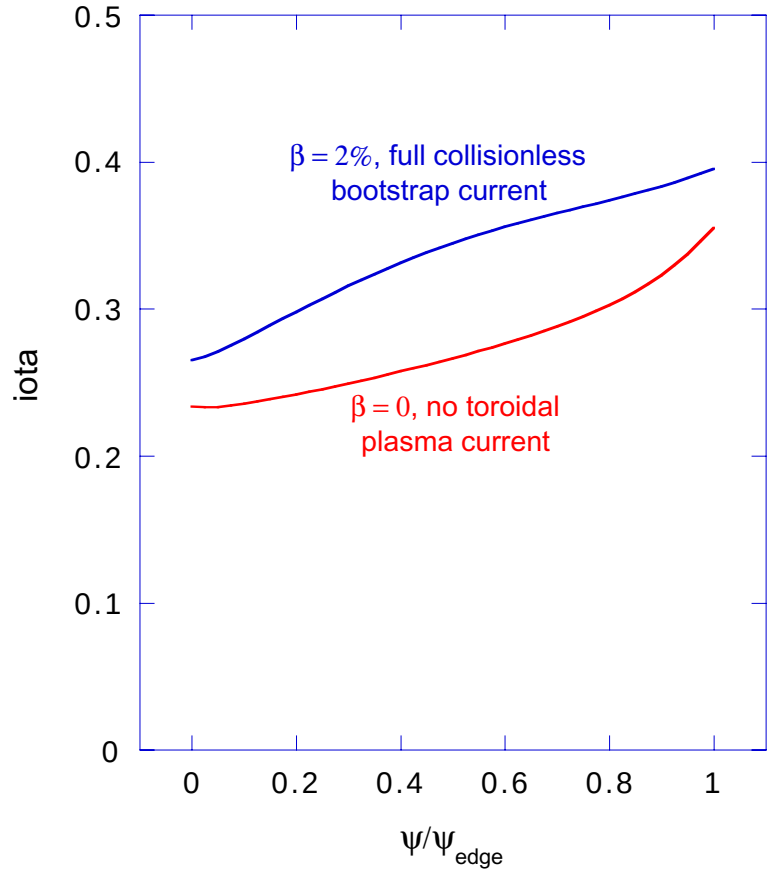

Figure 3. 13. Change in the ι(r) for the QPS reference configuration due to the bootstrap current.

bootstrap current is removed. In both cases the ι = 2/5 resonance is avoided, except possibly at the very edge of the plasma. At low ⟨β⟩, an Ohmically driven current can be used to approximate the equilibrium that is obtained with the bootstrap current, as shown in Chapter 7. Variation of the plasma current is also an important experimental parameter for studying current driven instabilities, island formation, and the effect of different values of rotational transform on transport. Studies of the influence of toroidal currents on plasma stability is of relevance to the higher ⟨β⟩ configurations which form the reactor vision of the QPS approach to compact stellarators.

3.4. An Improved Reference Configuration GB5

While the GB4 reference configuration fully satisfies the needs for the QPS CE-level experiment, an "updated" reference configuration (GB5) that is similar in appearance to the GB4 configuration, but with significantly improved low-ν* transport properties, has been found in the last two months that could supercede the reference GB4 configuration. Our analysis so far indicates that the GB5 configuration has similar stability properties as the GB4 configuration. While the GB5 configuration has not been analyzed yet for kink and vertical stability, we do not

expect it to be significantly different than for the GB4 configuration. We also expect the coils to be similar to those for GB4 based on the NESCOIL sheet current parameter. However, the GB4 modular coils have been optimized from a number of physics perspectives using free-boundary VMEC equilibria, and engineering analysis has been performed to assess the GB4 coil feasibility. This has not been done yet for the GB5 configuration, nor the same level of transport analysis. For these reasons we present GB4 as the reference QPS configuration, but it could be superceded by the GB5 configuration during the conceptual design phase. Where available, results for the GB5 configuration are compared with those for GB4 in the following chapters.

References

[1] S. P. Hirshman and J. C. Whitson, Phys. Fluids **26** 3553 (1983).

[2] S. P. Hirshman, K. C. Shaing, et al., Phys. Fluids, **29** (September, 1986); W. I. van Rij, S. P. Hirshman, Phys. Fluids B, **1** (March, 1989).

[3] R. Sanchez, S. P. Hirshman, J. C. Whitson, and A. S. Ware, J. Comput. Phys. 161, p 576 (2000).

[4] Merkel, P., Nuclear Fusion **27** (1987).

[5] A. H. Boozer, Phys. Fluids **24**, 1999 (1981).